Published in final edited form as:
Nanomedicine (Lond). 2009 June ; 4(4): 411–419. doi:10.2217/nnm.09.15.

Multicolor imaging of lymphatic function with two nanomaterials: quantum dot-labeled cancer cells and dendrimer-based optical agents

Hisataka Kobayashi[1], **Mikako Ogawa**[1], **Nobuyuki Kosaka**[1], **Peter L Choyke**[1], and **Yasuteru Urano**[2]

[1] Molecular Imaging Program, Center for Cancer Research, National Cancer Institute, NIH Bldg. 10, Room 1B40, MSC 1088, 10 Center Drive, Bethesda, MD 20892-1088, USA, Tel.: +1 301 435 4086; Fax: +1 301 402 3191; E-mail: kobayash@mail.nih.gov

[2] Graduate School of Pharmaceutical Sciences, The University of Tokyo, 7-3-1 Hongo, Bunkyo-ku, Tokyo 113-0033, Japan

Abstract

Aim—The lymphatics, critical conduits of metastases, are difficult to study because of their size and location. Two approaches to lymphatic imaging have been employed; cancer cell labeling provides information on cell migration and metastasis and macromolecular contrast agents enable visualization of the lymphatic drainage and identification of sentinel lymph node. Only one of these approaches is typically employed during an imaging examination. Here, we demonstrate the combined use of both approaches.

Method—In this study, we simultaneously visualize migration of quantum dot-labeled melanoma cells and the lymphatics using optically labeled dendrimers *in vivo*.

Results—The appropriate use of two nanomaterials, quantum dots and dendrimers, enabled the simultaneous tracking of cancer cells within draining lymphatics.

Conclusion—This technique could enable better understanding of lymph node metastasis.

Keywords

cancer; dendrimer; fluorescence; lymphatic flow; metastasis; multicolor imaging; quantum dot

Lymphatic invasion is an important route for metastasis of cancer. The lymphatic channels drain into sentinel lymph nodes, which are the first lymph nodes in a chain of nodes to receive the afferent lymphatics of the tumor bed. Therefore, sentinel lymph nodes are an expected site for cancer cell migration. Sentinel node identification has become an important procedure in patients with melanoma [1,2] and breast cancer [3]. Previous *in vivo* imaging techniques have

Correspondence to: Hisataka Kobayashi.

Ethical conduct of research
The authors state that they have obtained appropriate institutional review board approval or have followed the principles outlined in the Declaration of Helsinki for animal experimental investigations.

Financial & competing interests disclosure
The authors have no other relevant affiliations or financial involvement with any organization or entity with a financial interest in or financial conflict with the subject matter or materials discussed in the manuscript apart from those disclosed.

No writing assistance was utilized in the production of this manuscript.

employed nanosized molecules and particles, which enable the visualization of lymphatic drainage [4,5] and cell migration [6]. Cell labeling and lymphatic visualization are generally separate studies. However, the simultaneous noninvasive *in vivo* imaging of both cancer cell tracking and local lymphatic drainage with multicolor-fluorescence imaging has the potential to demonstrate the relationship between cell migration and lymphatic-drainage patterns.

Quantum dots (QDs) have superior brightness and do not photobleach, thus making them attractive agents for fluorescence labeling and long-term tracking of cancer cells [7]. However, QDs have the propensity to be endocytosed by cells, especially by macrophages in lymph nodes. Thus, QDs tend to be trapped by macrophages in the sentinel lymph node, remaining there for at least a week, and therefore are not useful for depicting lymphatic drainage distal to the sentinel node [8,9]. By contrast, dendrimer-based contrast agents, which are generally smaller than QDs and show minimal interaction with cells, are retained within the lymphatics, especially when their surface charge is modified with an appropriate coating or when conjugated to specific fluorophores [10–14]. Dendrimer-based contrast agents are retained within the lymphatics but are cleared from the sentinel lymph nodes within a day, enabling repeated injections. In addition, dendrimer-based contrast agents can be labeled with organic fluorophores (for optical imaging), radioisotopes (for scintigraphy) [14] and paramagnetic lanthanoid ions (for MRI) [12,15]. With appropriate combinations of nanomaterials, such as QDs and diethylene triamine pentaacetic acid (DTPA)-coated dendrimers, both lymphatic cell tracking and functional depiction of lymphatic drainage can be simultaneously visualized. Labeling with near-infrared (NIR) probes allows maximal transmission of light through tissue in order to enable minimally invasive imaging in live mice as well as *ex vivo* histological validation. In this study, we demonstrate *in vivo* cancer cell migration within the lymphatics by simultaneously visualizing QD-labeled melanoma cells within optically labeled lymphatics using fluorescent dendrimers in a mouse model.

Materials & methods

Chemicals

Carboxyl cadmium/selenium QDs, QD 655 ITK™ (peak emission wavelength at 655) and amino-reactive Alexa Fluor® 660, 700 and 750, and cyanine-based organic fluorescent dyes were purchased from Invitrogen Corporation (Carlsbad, CA, USA). Generation-6 polyamidoamine (PAMAM-G6) dendrimers with an ethylenediamine core, G6 interior, maximum 256 terminal primary amino groups and a molecular weight of 58.048 Da was purchased from Aldrich Chemical Co., (Milwaukee, WI, USA). 2-(p-isothiocyanatobenzyl)-DTPA (SCN-Bz-DTPA; ~700 Da) was purchased from Macrocyclic (Dallas, TX, USA).

Cells

B16, a human melanoma cell line, was obtained from the American Type Culture Collection. The B16 cell line was stably transfected with *CXCR4* as previously reported [16], selected by neomycin and cloned to create the B16CXCR4 cell line, which highly expresses the *CXCR4* gene and shows enhanced cell migration.

The B16CXCR4 cell was grown in Dulbecco's modified Eagle medium (DMEM; Life Technologies, Gaithersburg, MD, USA) containing 10% fetal bovine serum (FBS; Life Technologies), 0.03% L-glutamine (Life Technologies), 100 units/ml penicillin and 100 μg/ml streptomycin (Life Technologies) in 5% CO_2 at 37°C.

Synthesis & quality control of half DTPA-coated dendrimer-based NIR fluorescence contrast agents

Multicolor half DTPA-coated dendrimer-based NIR fluorescent contrast agents were synthesized using a method similar to one previously published [14]. Briefly, PAMAM-G6 was used for the basic platform structure; its solution, concentrated to 12 mg (210 nmol) in 2 ml of 0.1 M phosphate buffer, was reacted with 60 mg (~85 μmol) of SCN-Bz-DTPA at 40°C for 48 h at pH 8.5, coating half of the surface amine with DTPA and neutralizing surface charges. The resulting preparation was purified by diafiltration using the Centricon 30 (Amicon Co., Beverly, MA, USA).

The number of SCN-Bz-DTPA molecules conjugated per dendrimer was determined by a previously described ^{111}In-labeling assay [12]. Briefly, a 5 μl aliquot of the reaction mixture was reacted with ^{111}In chloride in 45 μl of 0.2 M sodium-acetate buffer at pH 4.2 for 1 h at room temperature. The radiolabeled sample was analyzed with size-exclusion high-performance liquid chromatography (equipped with a TSK G3000SWxL column, Tosoh Bioscience LLC, Montgomeryville, PA, USA; 0.067 M PB, 0.1 M KCl, pH 6.8; 1 ml/min) and an online radioactivity detector (Bioscan, Washington, DC, USA). The high-performance liquid chromatography profile showed 30% of the total ^{111}In-radioactivity was associated with the PAMAM-G6 fraction. Therefore, 122 SCN-Bz-DTPA molecules were conjugated per one PAMAM-G6 molecule.

Next, at room temperature, 2 mg (17 nmol) of G6-(Bz-DTPA)$_{122}$ in 400 μl of 0.3 M Na_2HPO_4 (pH 8.5) was rapidly mixed with 170 nmol (34 μl/5 mM) of either amino-reactive Alexa 660, 700 or 750-succinoimidyl ester solutions in dimethyl sulfoxide, and the reaction mixture was incubated for 15 min. The mixture was purified with Sephadex G-25 (Medium) (PD-10; GE Healthcare, Milwaukee, WI, USA).

The concentration of Alexa 660, 700 and 750 in each probe was measured by their absorption at 665, 703 and 753 nm, respectively, using the UV-visible spectroscopy (8453 Value UV-Vis system, Agilent Technologies, Palo Alto, CA, USA) to confirm the number of fluorophore molecules conjugated per G6 dendrimer molecule. The number of fluorophore molecules was 2.7, 3.3 and 2.9 for per G6-(Bz-DTPA)$_{122}$ Alexa 660, 700 and 750, respectively.

Cell labeling with QD655

Cell labeling was performed with a carboxyl QD655 (Invitrogen Corp.) using electroporation (GenPulseII, Bio-Rad Laboratories, Hercules, CA, USA). Briefly, 100 μl of the cell suspension, containing 2 million B16CXCR4 cells mixed with 400 nM of QD655, was placed in a 2 mm gap pulse cuvette (Bio-Rad Laboratories) and 150 V pulses were delivered after 500 cycles at 4°C. Immediately after electroporation, the cells were diluted to 5 ml in the culture media (DMEM, Gibco, Gaithersburg, MD, USA) containing 10% FBS (Gibco) and 0.03% L-glutamine and incubated for 30 min at 37°C. Labeled cells were repeatedly washed by completely eliminating unbound QD655 from the supernatant, which was confirmed by spectral fluorescence imaging (Maestro™ *In-Vivo* Imaging System, CRi Inc., Woburn, MA, USA).

As a control, we labeled cells with QD655 using a conventional endocytosis method. QD655 Qtracker® cell-labeling kit was purchased from Invitrogen Corp., which is used to monitor streptavidin-induced endocytosis of QDs. We incubated 2 million B16CXCR4 cells mixed with 20 nM of QD655 Qtracker in the same DMEM for 30 min at 37°C. The QD655-labeled cells were washed three times to eliminate the unbound QD655 Qtracker.

Validation of cell labeling

The fluorescence intensity of labeled cells was determined by macroscopic, microscopic and flow cytometry analysis. Immediately after the cells were washed the cell pellet was imaged by spectral fluorescence imaging (Maestro). Then 10 μl of cell suspension was examined by a fluorescence microscopic system (BX61, Olympus America Inc., Center Valley, PA, USA), with an excitation/emission filter set of 530–570 nm band pass and 590 nm long pass, respectively. Next, the fluorescence intensity of each cell was measured by flow cytometry (FACSCalibur™ flow cytometer, Becton Dickinson, Franklin Lakes, NJ, USA) using 488 nm excitation laser and 650 long pass emission filters.

In addition, to validate the electroporation technique for cell labeling, cell labeling was performed with the same protocol shown earlier with different QD655 concentrations, 0, 4, 10, 40, 100 and 400 nM. Labeled cells were analyzed by flow cytometry at the same settings.

Cell tracking study

All *in vivo* procedures were carried out in compliance with the Guide for the Care and Use of Laboratory Animal Resources (1996), National Research Council, and approved by the National Cancer Institute Animal Care and Use Committee. Immediately after the cells had been washed, and the cell-labeling efficacy validated, cells were suspended in phosphate-buffered saline at 20 million/ml and injected as a 50 μl solution into the lower lip of 8–10-week-old female nude mice.

In vivo multiple excitation spectrally resolved four-color fluorescence imaging

Simultaneous cell tracking and lymphatic flow imaging was performed either 6 or 24 h after injection of QD655-labeled B16CXCR4 cells (n = 4 in each group). Lymphatic flow imaging was performed with serial intradermal injections of the half-coated G6 dendrimer-based Alexa 660 agent in the right ear, the half-coated G6 dendrimer-based Alexa 700 in the left ear and the half-coated G6 dendrimer-based Alexa 750 in the lower lip, where QD655-labeled B16CXCR4 cells were injected. All dendrimer-based contrast agents were serially injected 5 min before the images were taken. Multiple excitation spectral fluorescence imaging was performed with sequential filter sets (green: excitation 503–555 nm band pass, emission 580 nm long pass; deep red: excitation 671–705 nm band pass, emission 750 nm long pass). Animals were placed in the supine position whilst under pentobarbital anesthesia. The injection sites were masked with a nonfluorescent black tape because the signal from the injection site would otherwise overwhelm the dynamic range of the camera, rendering the unmixing algorithm nonfunctional. After obtaining *in vivo* images, lymphadenectomy was performed and another spectral fluorescence image was obtained intra-operatively. All of the removed lymph nodes were validated by *exvivo* spectral fluorescence imaging. The tunable filter was automatically stepped in 10-nm increments from 600 to 950 nm for both filter sets, using the 10:1 exposure time for images captured with green and deep red filter sets at each wavelength. Each acquisition with this two-excitation spectral fluorescence imaging technique took approximately 2 min. Collected images were analyzed by the Maestro software (Nuance™ Ver 2.4, CRi, Inc.), which uses multispectral unmixing algorithms to separate autofluorescence from QD655 and NIR dye signals. A composite image consisting of all four fluorescent signals and autofluorescence was generated using a spectral library obtained from each lymph node injected with either G6-$(Bz\text{-}DTPA)_{122}$-$(NIR)_4$ or QD655 solutions.

Results

Validation of cell labeling

For cell tracking we employed a melanoma cell line, B16CXCR4, that has been stably transfected with the chemokine receptor *CXCR4* gene to a parental B16 melanoma cell line [16]. The presence of CXCR4 enhances *in vivo* cell migration leading to early metastases [17]. Cell labeling was performed with a carboxyl cadmium-selenium QD (QD655; peak emission: 655 nm) using an electroporation technique. After repeatedly washing the cell to eliminate unbound QD655, cells were suspended in phosphate-buffered saline at 20 million/ml and injected as a 50 μl of cell solution into the lower lip of 8–10-week-old female nude mice. The fluorescence intensity of each cell was measured by flow cytometry and increased as the concentration of QD655 in the cell suspension increased (Figure 1A). QD655 was diffusely distributed in the cytoplasm of B16CXCR4 cells (Figure 1B). Scattered QD655-labeled cells were bright enough to be visualized with a macroscopic spectral fluorescence animal imager (Figure 1C).

Multicolor *in vivo* lymphatic functional imaging

For lymphatic imaging, three different NIR-labeled PAMAM G6 half DTPA-coated dendrimers were synthesized with Alexa 660, 700 and 750, and SCN-Bz-DTPA using similar methods to those previously reported [14]. Simultaneous cell tracking and lymphatic flow imaging was performed 6 and 24 h after injection of QD655-labeled B16CXCR4 cells. Lymphatic imaging was performed with serial intradermal injections of DTPA-coated dendrimer-bound G6-Alexa 660 agent in the right ear, G6-Alexa 700 in the left ear and G6-Alexa 750 in the lower lip, where QD655-labeled B16CXCR4 cells were injected. Multiple excitation spectral fluorescence imaging was performed with two sequential filter sets (green: excitation 503–555 nm band pass, emission 580 nm long pass; deep red: excitation 671–705 nm band pass, emission 750 nm long pass). After obtaining *in vivo* images, a lymphadenectomy was performed and another spectral fluorescence image was obtained during surgery. All removed lymph nodes were confirmed by *ex vivo* spectral fluorescence imaging. Spectral fluorescence imaging at 6 h postinjection of QD655-labeled B16CXCR4 cells depicted a clear signal from the proximal rim of the superficial cervical lymph nodes (Figure 2A) and a weaker, diffuse homogeneous signal from the same lymph nodes 24 h postinjection (Figure 2B).

The different lymphatic drainages of the neck were clearly visualized with distinct colors in all mice (Figure 2). The lymph nodes, which showed the strongest QD655 signal at 6 h postinjection, demonstrated the greatest drainage from the injection site. Spectral fluorescence imaging during surgery showed that the QD655 signal emanated only from the proximal rim of the sentinel lymph node with regard to the injection site of QD655-labeled B16CXCR4 cells (Figures 2A & 3C). Microscopic fluorescence images of the frozen sections of respective lymph nodes directly corresponded to the *in vivo* and intraoperative imaging (Figure 3). In the lymph nodes, the appearance of QD655-labeled B16CXCR4 cells coincided at the rim (subcapsular sinus) and the travecula with the visualization of lymphatic flow at 6 h postinjection (Figure 3A & C), but by 24 h they were diffusely distributed within the lymph node and located more in the follicles which were further away from the lymphatic drainage than the travecula (Figure 3B & D). QD655-labeled B16CXCR4 cells also migrated to the secondary draining lymph nodes 24 h after injection as detected by *in vivo* imaging (Figure 2B) and validated in Figure 4.

Discussion

Cell labeling for lymphatic imaging poses a challenge. A common method of cell labeling is to genetically label cells with endogenous fluorescent proteins. Fluorescent proteins are

excellent endogenous fluorescence emitters [18,19], but must be transfected into cells, which makes them unlikely to be permitted for use in humans in the near future [20]. An alternative cell-labeling method uses exogenous fluorescent probes and labels the cells via endocytosis (or pinocytosis). Endocytosis is the biological process whereby the cell engulfs the exogenous fluorescent materials in the endolysosome (Supplementary Figure 1A) (see online www.futuremedicine.com/toc/nnm/4/4). Endocytosis is relatively easy to induce and can be accomplished quickly (within 1 h) in most cancer cells. The fluorescence yield is comparable with cell labeling using endogenous fluorescent proteins [21]. By using transfection reagents including cationic liposomes, dendrimers, streptavidin and Tat-peptides, pinocytosis can be accelerated, resulting in highly efficient cell labeling. However, degradation of the engulfed nanoparticle (e.g., iron oxides) occurs in the lysosome after endo/pinocytosis and could affect the stability of some fluorophores [22]. Another cell-labeling method is electroporation, wherein electric currents cause mechanical loosening of the cell membrane allowing exogenous fluorescent materials into the cytoplasm, where the chemical environment is less harsh. The electroporation method has recently been used for cell labeling with various nanomaterials [23–25]. Since cell labeling with electroporation is caused by passive diffusion, the cell-labeling efficacy with electroporation is lower than the method employing endocytosis (Supplementary Figure 1B), but has the advantage of more precise control because the process is concentration dependent (Figure 1). Nevertheless, electroporation can temporally loosen the cell membranes and damage the intracellular integrity, a process that typically recovers within 4 h (Supplementary Figure 2). For short-term imaging experiments, QDs with organic NIR fluorophores can be used as an alternative to QDs. However, since QDs are highly resistent to photobleaching and biodegradation, cell labeling with QDs is expected to last longer and to be preserved even during histologic analysis. However, in any particular cell type, either electroporaton or endocytosis might be preferable [26]. The appropriate subcellular localization of nanomaterials for cell labeling might help to minimize the toxicity from heavy metals such as cadmium and gadolinium which can be found in QDs or MRI contrast agents [25,27].

We demonstrate the simultaneous visualization of metastatic cells within enhanced lymphatics using multicolor imaging. Dendrimers were chosen to visualize the lymphatics since nanosized particles and molecules are normally drained by the lymphatic system, and interstitial injection of contrast agents with high molecular weights results in visualization of the lymphatic vessels [4,28]. Similarly, successful dendrimer-based agents have been labeled with radionuclides [14], paramagnetic lanthanides [5,29] and fluorophores, singly or in combination [30]. Prior results with gadolinium-labeled dendrimer-based contrast agents suggest that relatively large nanoparticles (~10 nm diameter) were optimal for visualizing regional lymphatics following intracutaneous injection [29,31]. Carboxyl QDs, which are in the optimal hydrodynamic size range for lymphatic imaging, were trapped more efficiently by macrophages than surface-coated dendrimer-based reagents and therefore might require surface modification to evade phagocytosis, although the modification would alter the size of the QDs and potentially compromise their ability to enter the lymphatics. In reality, carboxyl QDs did not show a noticeable washout from the first draining (sentinel) lymph node for up to 3 h postinjection with intense uptake by macrophages, but rarely depicted secondary draining lymph nodes [8, 9]. By contrast, NIR-labeled IgG and gadolinium-labeled fully-coated dendrimer showed peak accumulation within 1 h postinjection and complete washout from the brightest lymph node within 1 day [32,33]. Therefore, QDs stayed in the first draining lymph node longer than NIR dye-labeled IgG or surface-coated dendrimers with similar hydrodynamic sizes. In addition, the multiple excitation spectral fluorescence imaging technique enabled us to perform multicolor imaging with good sensitivity using multiple organic NIR fluorescent dyes similar to QDs. Overall, surface-coated dendrimer-based NIR fluorescence contrast agents are an appropriate choice for lymphatic functional imaging.

Conclusion

Each nanomaterial displays different physical, chemical, biological and pharmacological characteristics, which can be harnessed for specific applications. Here, we demonstrate that combining two nanoparticles has the potential to simultaneously track cancer cells as well as visualize local lymphatic function. This may enable study of the physiological mechanisms underlying lymphatic metastases for basic cancer research. In addition, this finding can provide evidence that dendrimer-based lymphatic imaging can correctly depict the sentinel lymph nodes, which may ultimately have a clinical application.

Future perspective

The lymphatic system is a complex network of lymph vessels, lymphatic organs and lymph nodes. Traditionally, imaging of the lymphatic system has been based on conventional clinical imaging methods such as CT, MRI and PET, and ultrasound. None of these techniques are capable of detecting both lymphatic drainage patterns and lymph nodes. Interstitial injection of radiolabeled nanoparticles (lymphoscintigraphy) has the disadvantage of poor resolution and is unable to simultaneously visualize multiple lymphatic functions: lymphatic drainage and cell migration. Therefore, this multicolor optical imaging method using two nanomaterials could help our understanding of how cells metastasize to lymph nodes and how the lymphatics facilitate this. In addition, since this optical imaging method can be performed relatively inexpensively, the method could, in part, be translated to the clinic, especially for the diagnosis and treatment of lymphatic metastasis from melanoma and breast cancer.

Executive summary

- Both pinocytosis and electroporation efficiently label melanoma cells with quantum dots (QDs).
- The electroporation method was able to precisely control labeling of melanoma cells by adjusting the concentration of QDs.
- The electroporation cell-labeling method resulted in cytoplasmic accumulation of QDs which may be preferable to endolysosomes with their harsher chemical environment.
- Dendrimer contrast agents were used to simultaneously visualize multiple lymphatic drainages to the sentinel lymph nodes in distinct colors.
- Melanoma cells initially migrated along the lymphatic draining flows into the sentinel lymph nodes.
- Melanoma cells migrated away from the lymphatic draining flows and stayed in the lymph node cortex for 1 day after injection.
- Melanoma cells migrated along the lymphatic vessels into the secondary lymph nodes 1 day after injection.
- Multicolor imaging with two distinct nanomaterials enabled the simultaneous visualization of both melanoma cell migration and lymphatic drainage into sentinel and secondary lymph nodes.
- This imaging technique could be a useful tool in developing a better understanding of how cells metastasize to lymph nodes and how the lymphatics facilitate this process.

Supplementary Material

Refer to Web version on PubMed Central for supplementary material.

Acknowledgments

This research was supported by the Intramural Research Program of the NIH, National Cancer Institute, Center for Cancer Research, USA.

Bibliography

Papers of special note have been highlighted as:

▪ of interest

1. Cochran AJ, Ohsie SJ, Binder SW. Pathobiology of the sentinel node. Curr Opin Oncol 2008;20(2): 190–195. [PubMed: 18300769]

2. Cook MG, Di Palma S. Pathology of sentinel lymph nodes for melanoma. J Clin Pathol 2008;61(8): 897–902. [PubMed: 18515403]

3. Sato K, Shigenaga R, Ueda S, Shigekawa T, Krag DN. Sentinel lymph node biopsy for breast cancer. J Surg Oncol 2007;96(4):322–329. [PubMed: 17879334]

4▪. Kim S, Lim YT, Soltesz EG, et al. Near-infrared fluorescent type II quantum dots for sentinel lymph node mapping. Nat Biotechnol 2004;22(1):93–97. Initial work on lymphatic optical imaging with quantum dots. [PubMed: 14661026]

5▪. Kobayashi H, Kawamoto S, Star RA, Waldmann TA, Tagaya Y, Brechbiel MW. Micro-magnetic resonance lymphangiography in mice using a novel dendrimer-based magnetic resonance imaging contrast agent. Cancer Res 2003;63(2):271–276. Initial work on lymphatic MRI using dendrimer-based contrast agent. [PubMed: 12543772]

6. Voura EB, Jaiswal JK, Mattoussi H, Simon SM. Tracking metastatic tumor cell extravasation with quantum dot nanocrystals and fluorescence emission-scanning microscopy. Nat Med 2004;10(9):993–998. [PubMed: 15334072]

7. Jaiswal JK, Mattoussi H, Mauro JM, Simon SM. Long-term multiple color imaging of live cells using quantum dot bioconjugates. Nat Biotechnol 2003;21(1):47–51. [PubMed: 12459736]

8. Hama Y, Koyama Y, Urano Y, Choyke PL, Kobayashi H. Simultaneous two-color spectral fluorescence lymphangiography with near infrared quantum dots to map two lymphatic flows from the breast and the upper extremity. Breast Cancer Res Treat 2007;103(1):23–28. [PubMed: 17028977]

9. Kobayashi H, Hama Y, Koyama Y, et al. Simultaneous multicolor imaging of five different lymphatic basins using quantum dots. Nano Lett 2007;7(6):1711–1716. [PubMed: 17530812]

10. Kono K, Kojima C, Hayashi N, et al. Preparation and cytotoxic activity of poly(ethylene glycol)-modified poly (amidoamine) dendrimers bearing adriamycin. Biomaterials 2008;29(11):1664–1675. [PubMed: 18194811]

11. Kojima C, Kono K, Maruyama K, Takagishi T. Synthesis of polyamidoamine dendrimers having poly(ethylene glycol) grafts and their ability to encapsulate anticancer drugs. Bioconjug Chem 2000;11(6):910–917. [PubMed: 11087341]

12▪. Kobayashi H, Sato N, Hiraga A, et al. 3D-micro-MR angiography of mice using macromolecular MR contrast agents with polyamidoamine dendrimer core with reference to their pharmacokinetic properties. Magn Reson Med 2001;45(3):454–460. Initial work on vascular MRI using dendrimer-based contrast agent. [PubMed: 11241704]

13. Sato N, Kobayashi H, Saga T, et al. Tumor targeting and imaging of intraperitoneal tumors by use of antisense oligo-DNA complexed with dendrimers and/or avidin in mice. Clin Cancer Res 2001;7 (11):3606–3612. [PubMed: 11705883]

14▪. Kobayashi H, Koyama Y, Barrett T, et al. Multi-modal nano-probes for radionuclide and 5-color near infrared optical lymphatic imaging. ACS Nano 2007;1(4):258–264. Important work on simultaneous multicolor lymphatic optical/nuclear imaging using dendrimer-based dual-modal contrast agents. [PubMed: 19079788]

15▪. Barrett T, Choyke PL, Kobayashi H. Imaging of the lymphatic system: new horizons. Contrast Media Mol Imaging 2006;1(6):230–245. Excellent review of lymphatic imaging. [PubMed: 17191764]

16. Kakinuma T, Nadiminti H, Lonsdorf AS, et al. Small numbers of residual tumor cells at the site of primary inoculation are critical for anti-tumor immunity following challenge at a secondary location. Cancer Immunol Immunother 2007;56(7):1119–1131. [PubMed: 17139493]

17. Cardones AR, Murakami T, Hwang ST. CXCR4 enhances adhesion of B16 tumor cells to endothelial cells *in vitro* and *in vivo* via β(1) integrin. Cancer Res 2003;63(20):6751–6757. [PubMed: 14583470]

18. Hasegawa S, Yang M, Chishima T, et al. *In vivo* tumor delivery of the green fluorescent protein gene to report future occurrence of metastasis. Cancer Gene Ther 2000;7(10):1336–1340. [PubMed: 11059691]

19▪. Hoffman RM. The multiple uses of fluorescent proteins to visualize cancer *in vivo*. Nat Rev Cancer 2005;5(10):796–806. Important work on multicolor optical imaging using more than one fluorescent protein concurrently. [PubMed: 16195751]

20. Yang M, Baranov E, Jiang P, et al. Whole-body optical imaging of green fluorescent protein-expressing tumors and metastases. Proc Natl Acad Sci USA 2000;97(3):1206–1211. [PubMed: 10655509]

21. Gilad AA, Walczak P, McMahon MT, et al. MR tracking of transplanted cells with “positive contrast” using manganese oxide nanoparticles. Magn Reson Med 2008;60(1):1–7. [PubMed: 18581402]

22. Hayashi K, Jiang P, Yamauchi K, et al. Real-time imaging of tumor-cell shedding and trafficking in lymphatic channels. Cancer Res 2007;67(17):8223–8228. [PubMed: 17804736]

23. Arbab AS, Wilson LB, Ashari P, Jordan EK, Lewis BK, Frank JA. A model of lysosomal metabolism of dextran coated superparamagnetic iron oxide (SPIO) nanoparticles: implications for cellular magnetic resonance imaging. NMR Biomed 2005;18(6):383–389. [PubMed: 16013087]

24. Walczak P, Kedziorek DA, Gilad AA, Lin S, Bulte JW. Instant MR labeling of stem cells using magnetoelectroporation. Magn Reson Med 2005;54(4):769–774. [PubMed: 16161115]

25. Terreno E, Geninatti Crich S, Belfiore S, et al. Effect of the intracellular localization of a Gd-based imaging probe on the relaxation enhancement of water protons. Magn Reson Med 2006;55(3):491–497. [PubMed: 16450336]

26. Rosen AB, Kelly DJ, Schuldt AJT, et al. Finding fluorescent needles in the cardiac haystack: tracking human mesenchymal stem cells labeled with quantum dots for quantitative *in vivo* three-dimensional fluorescence analysis. Stem Cells 2007;25(8):2128–2138. [PubMed: 17495112]

27. Cho SJ, Maysinger D, Jain M, Roder B, Hackbarth S, Winnik FM. Long-term exposure to CdTe quantum dots causes functional impairments in live cells. Langmuir 2007;23(4):1974–1980. [PubMed: 17279683]

28. Kobayashi H, Brechbiel MW. Dendrimer-based nanosized MRI contrast agents. Curr Pharm Biotechnol 2004;5(6):539–549. [PubMed: 15579043]

29. Kobayashi H, Kawamoto S, Sakai Y, et al. Lymphatic drainage imaging of breast cancer in mice by micro-magnetic resonance lymphangiography using a nano-size paramagnetic contrast agent. J Natl Cancer Inst 2004;96(9):703–708. [PubMed: 15126607]

30. Koyama Y, Talanov VS, Bernardo M, et al. A dendrimer-based nanosized contrast agent dual-labeled for magnetic resonance and optical fluorescence imaging to localize the sentinel lymph node in mice. J Magn Reson Imaging 2007;25(4):866–871. [PubMed: 17345640]

31. Kobayashi H, Kawamoto S, Choyke PL, et al. Comparison of dendrimer-based macromolecular contrast agents for dynamic micro-magnetic resonance lymphangiography. Magn Reson Med 2003;50(4):758–766. [PubMed: 14523962]

32. Kobayashi H, Kawamoto S, Bernardo M, Brechbiel MW, Knopp MV, Choyke PL. Delivery of gadolinium-labeled nanoparticles to the sentinel lymph node: comparison of the sentinel node visualization and estimations of intra-nodal gadolinium concentration by the magnetic resonance imaging. J Control Release 2006;111(3):343–351. [PubMed: 16490277]

33. Hama Y, Koyama Y, Urano Y, Choyke PL, Kobayashi H. Two-color lymphatic mapping using Ig-conjugated near infrared optical probes. J Invest Dermatol 2007;127(10):2351–2356. [PubMed: 17522707]

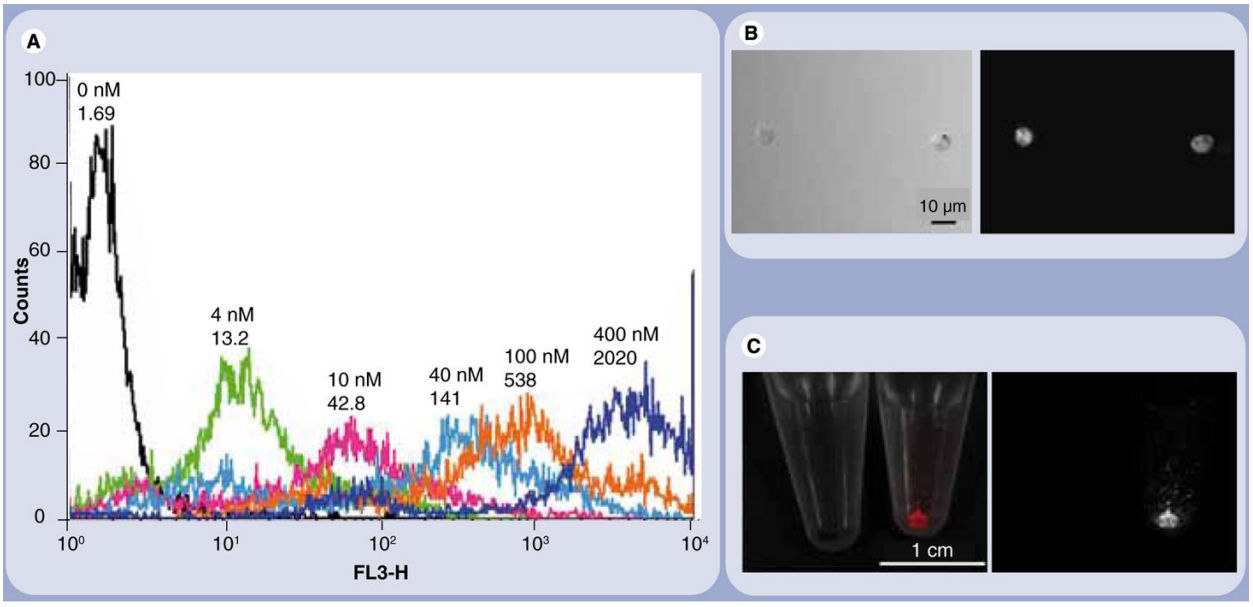

Figure 1. Quantum dots label B16CXCR4 cells in a concentration-dependent manner

(A)A histogram chart of a flow cytometry and **(B)** microscopic and **(C)** macroscopic fluorescence images of quantum dot (QD)655-labeled B16CXCR4 cells are shown. B16CXCR4 cells are efficiently labeled with the QD655 concentration dependently shown in the flow cytometry **(A)**. The labeled cells emit bright fluorescence under the microscope (**(B)** 50 ms image) as well as in a macroscopic image (**(C)** 10 ms image).

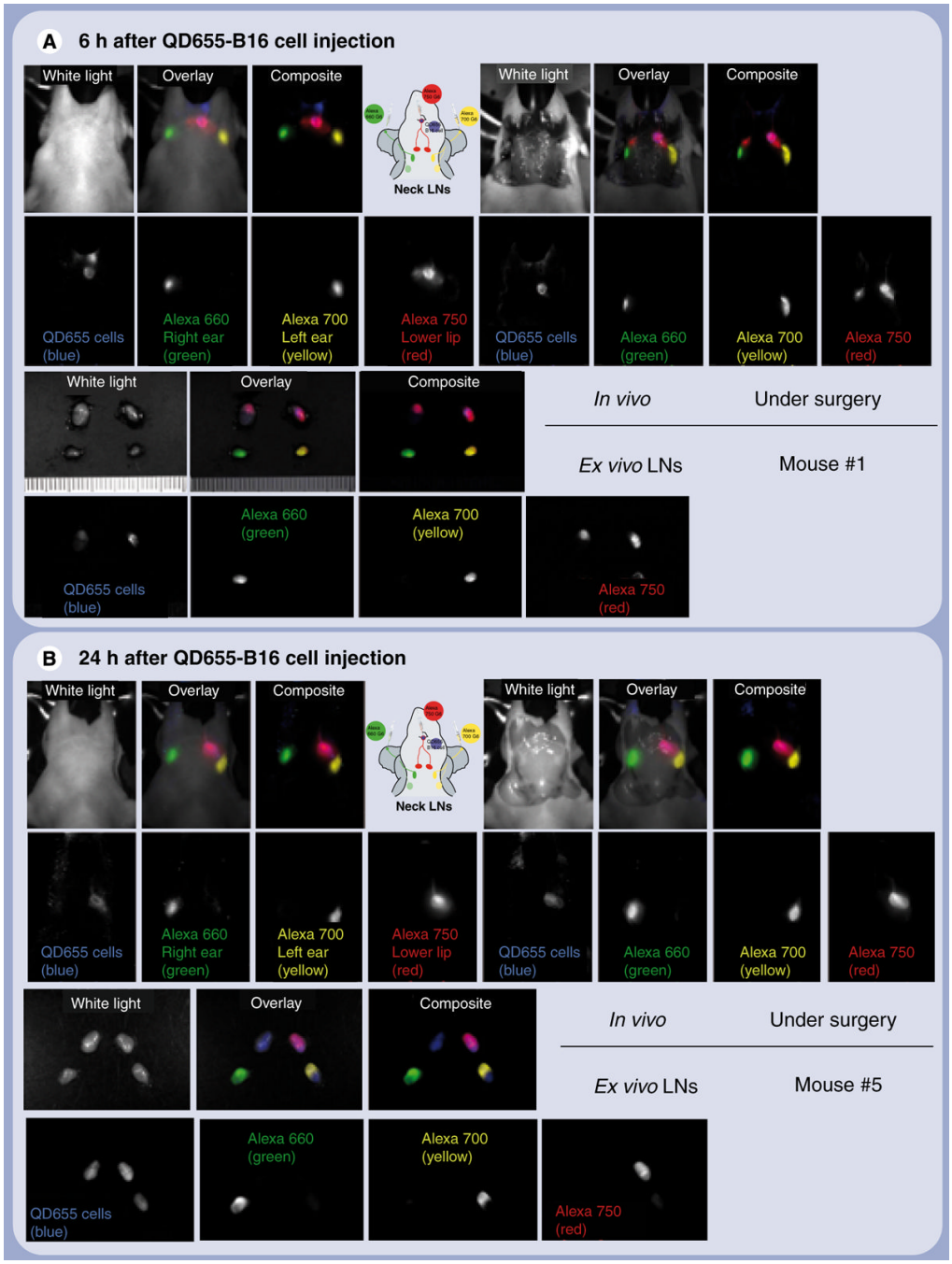

Figure 2. Simultaneous fluorescence imaging of quantum dot 655-labeled B16CXCR4 melanoma cells migrating into lymph nodes and lymphatic drainage demonstrating that cancer cells migrate along local lymphatic channels before invading the lymph nodes

(A) 6 h after injection of B16CXCR4 cells. **(B)** 24 h after injection of B16CXCR4 cells. QD655 signal from B16CXCR4 cells is shown in blue. The lymphatic flows from the right and left ears, and the lower lip in which B16CXCR4 cells were injected are shown in green, yellow and red, respectively. The part of the superficial cervical neck lymph node shown in pink represents the mixed color of blue and red where colocalized B16CXCR4 cells (blue) and the lymphatic flow from the lower lip (red) coincide. Images of one mouse in each group are shown.

Similar images were obtained from the other three mice in each group. LN: Lymph node; QD: Quantum dot.

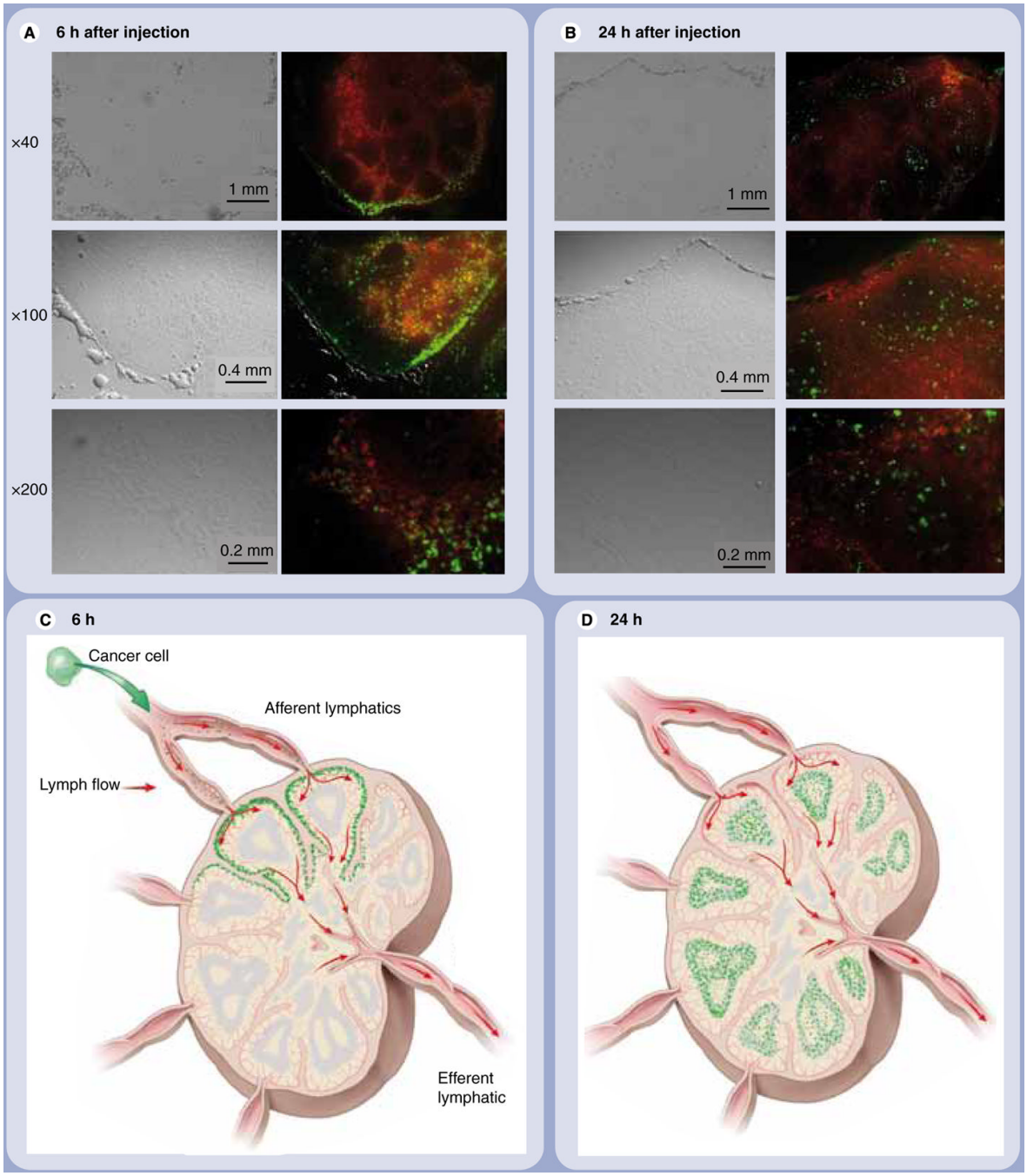

Figure 3. Fluorescence microscopy demonstrating peripheral enhancement followed by diffuse enhancement

(A) 6 h after injection of B16CXCR4 cells. **(B)** 24 h after injection of B16CXCR4 cells. Quantum dot (QD)655 signal from B16CXCR4 cells is shown in green. All lymphatic flows are shown in red. At 6 h after injection of B16CXCR4 cells, the majority of QD655-labeled B16CXCR4 melanoma cells are located at the proximal rim (subcapsular sinus) of the superficial cervical neck lymph node to the lower lip. Scattered QD655-labeled B16CXCR4 are also found in the travecula, colocalized with the lymphatic flow. At 24 h after injection of cells, the QD655-labeled B16CXCR4 cells diffusely distributed in the entire sentinel lymph node and located in higher quantities in the follicles, which are further away from the lymphatic

flows (depicted with dendrimer-based lymphatic flow agents in red) than the subcapsular sinus and the travecula. To facilitate the understanding of microscopic images, schemas of *in vivo* lymphatic flow and cell migration are shown. **(C)** 6 h after injection of B16CXCR4 cells. **(D)** 24 h after injection of B16CXCR4 cells. Cells are shown in green and the lymphatic flows are shown with red arrows.

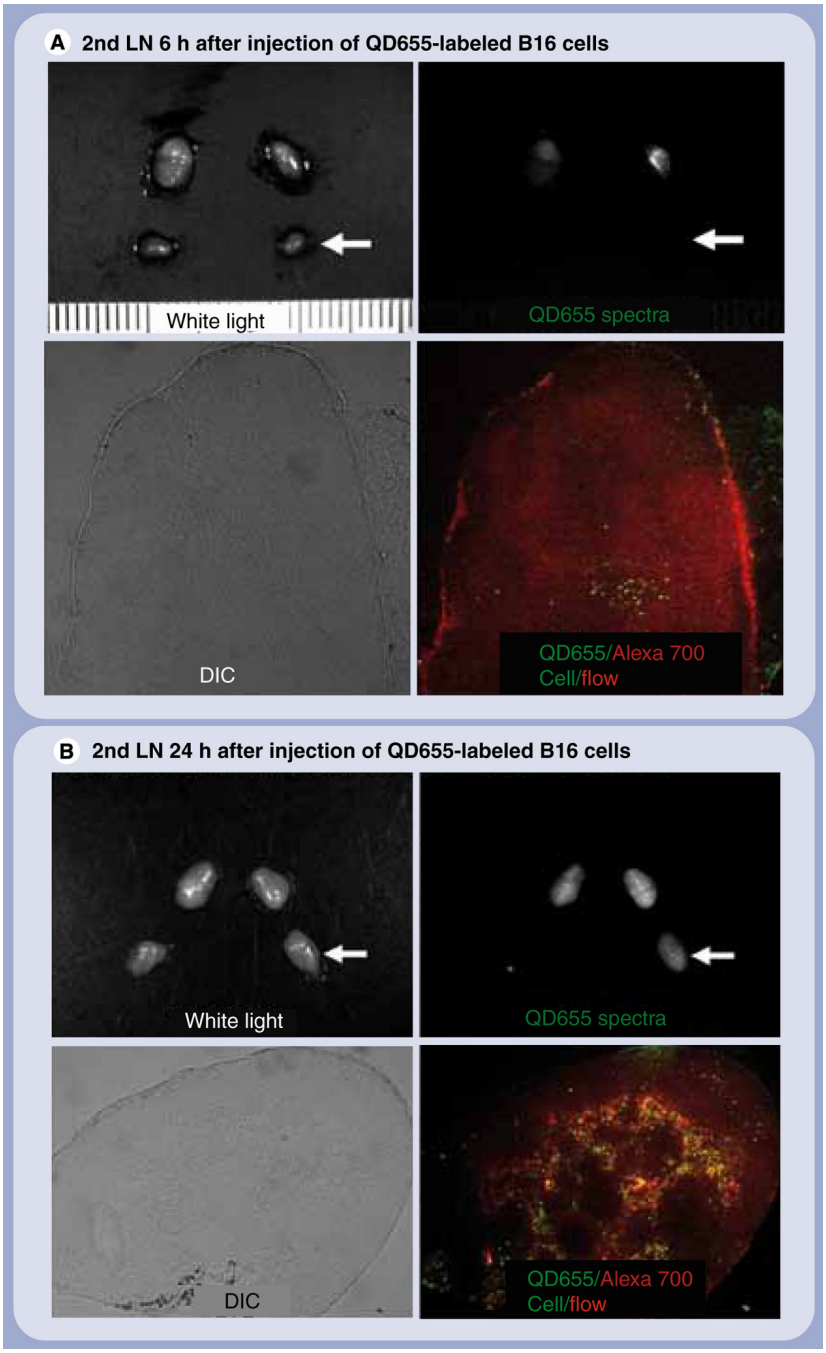

Figure 4. Cell migration to the secondry draining lymph nodes

(A) The secondary draining sentinel LN (the left deep neck LN; arrows) did not show a QD655 signal from B16CXCR4 cells in an *ex vivo* LN macro-image at 6 h after injection and contained small numbers of scattered QD655-labeled cells (green), which were shown in a microscopic image of the frozen section (**(A)** ×40). **(B)** By contrast, the same LN showed a QD655 signal from B16CXCR4 cells in an *ex vivo* LN macro-image at 24 h postinjection and contained a large number of QD655-labeled cells (green) migrated mostly along with the lymphatic flow (red), which were shown in a microscopic image of the frozen section (**(B)** ×40). LN: Lymph node; QD: Quantum dot.